Z dependence of $K\alpha$ x-ray satellite structure in heavy-ion–atom collisions*

R. L. Watson, F. E. Jenson, and T. Chiao
Department of Chemistry and Cyclotron Institute, Texas A & M University, College Station, Texas 77843
(Received 3 June 1974)

The spectra of $K\alpha$ x rays emitted as a result of heavy-ion–atom collisions have been measured with a Bragg spectrometer using a variety of equal velocity (1.7 MeV/amu) heavy ions ranging from $_1$H to $_{18}$Ar incident on solid targets containing atoms of $_{13}$Al, $_{17}$Cl, and $_{19}$K. In the cases of Cl and K, the measured $K\alpha_{1,2}$-$K\alpha$ satellite energy differences for one through seven L-shell vacancies were found to be systematically larger than those calculated using the Herman-Skillman Hartree-Fock-Slater program. Values of the binomial probability parameter obtained by fitting the relative satellite intensities with binomial distributions have been compared to theoretical values calculated using an impact-parameter formulation of the binary-encounter approximation. In the Al spectra obtained with S and Ar ions, the $K\alpha_{1,2}$ peak is observed to have an intensity six to seven times larger than is expected on the basis of a binomial fit to the satellite peaks.

I. INTRODUCTION

Numerous studies of ion-atom collisions have been reported in which it has been shown that K-shell ionization is usually accompanied by multiple L-shell ionization when heavy charged particles are used as projectiles.[1] In particular, measurements with high-resolution crystal spectrometers have revealed the presence of intense satellite lines in the spectra of $K\alpha$ x rays produced as a result of the collision process. Based upon comparisons with calculated energies, these satellite lines have been attributed to $K\alpha$ x-ray emission from atoms having one or more L-shell vacancies. Detailed analyses of the $K\alpha$ satellite spectra for Al excited by nitrogen ions, and by oxygen, fluorine, and chlorine ions, and for Fe, Si, and Mg excited by oxygen ions are given in Refs. 2, 3, 4, 5, and 6, respectively.

It was first noted by Burch and Swanson[7] that the intensity patterns of the $K\alpha$ satellite lines resulting from oxygen-ion bombardments are well represented by binomial distributions. This fact implies that correlation effects are relatively unimportant in the multiple L-shell ionization process and enables a convenient characterization of the satellite spectrum in terms of a binomial probability parameter which is related to the average L-shell ionization probability *per electron* for K-shell ionizing collisions. The velocity dependence of the simultaneous K- plus L-shell ionization probability has been investigated by a number of workers[8–10] and found to reflect the velocity dependence of the cross section for L-shell ionization by Coulomb excitation. However, rather large differences in magnitude between measured multiple-ionization probabilities and those calculated using binary-encounter approximation (BEA) descriptions of the multiple ionization process were found. It is therefore of interest to study further the various features of simultaneous K- plus L-shell ionization in heavy-ion–atom collisions.

The present work has been carried out for the purpose of (i) providing additional $K\alpha$ x-ray satellite energy data, and (ii) investigating in detail the dependence of $K\alpha$ x-ray satellite intensities on projectile and target atomic number. Spectral measurements have been performed for Al, Cl, and K $K\alpha$ x-ray production by equal velocity projectiles (1.7 MeV/amu) of H, He, C, O, Ne, S, and Ar ions using a Bragg-crystal spectrometer.

II. EXPERIMENTAL METHODS

A. Ion beams and targets

The Texas A & M variable-energy cycloton was used to accelerate beams of 3.4-MeV $^2H^+$, 6.7-MeV $^4He^+$, 22.0-MeV $^{12}C^{+3}$, 32.3-MeV $^{16}O^{+2}$, 40.5-MeV $^{20}Ne^{+3}$, 64.6-MeV $^{32}S^{+4}$, and 81.0-MeV $^{40}Ar^{+5}$. At these energies, the average charge states of the H, He, C, and O ions in solid targets are estimated to be +1, +2, +5.5, and +7.2, respectively.[11] The charge-state distribution for 81.0-MeV Ar ions emerging from a 125-μg/cm^2 Al foil was experimentally determined and the average charge state found to be +13.6.

The target thicknesses were chosen such that the various projectiles all had an energy of 1.7 ± 0.1 MeV/amu at the average depth for the detection of the $K\alpha$ x rays. In determining the appropriate target thicknesses, account was taken of the projectile rate of energy loss and the variation of x-ray production cross section with energy, as well as the absorption of the emitted x rays as a function of target depth. The targets ranged in

thickness from 1.0 to 2.2 mg/cm^2 (corrected for the 45° inclination angle). Self-supporting metallic Al foils were used as targets in the Al measurements while NaCl and KCl targets vacuum evaporated onto 1.4 mg/cm^2 Al backings were used in the Cl and K measurements, respectively.

B. Spectrometer

The crystal spectrometer used in these studies was constructed from a design obtained from the Naval Research Laboratory[12] and was essentially identical to the spectrometer used by Burkhalter *et al.*[13] and Knudson *et al.*[2] in previous measurements of ion-induced x-ray spectra. It employs flat-crystal x-ray optics and operates in a step-scanning mode. Additional modifications to the system were made to allow adjustment of the Bragg crystal and the entrance soller slit alignments by remote control.

The spectrometer was positioned perpendicular to the incident ion beam and targets were mounted at 45° with respect to both the ion beam and the spectrometer. Collimation of the incident x rays was accomplished by means of a set of commercial soller slits which limited the angular dispersion to approximately 0.3°. Bragg crystals of PET (pentaerythritol), NaCl, and LiF were used for the Al, Cl, and K measurements, respectively. The detector was a gas-flow proportional counter (P-10 gas) with a grid-supported 4-μm aluminized Mylar window. The experimental energy resolution full width at half-maximum (FWHM) using He ions as projectiles was 3.3 eV for the Al $K\alpha_{1,2}$ peak, 9.4 eV for the Cl $K\alpha_{1,2}$ peak, and 9.7 eV for the K $K\alpha_{1,2}$ peak.

Automatic control of the spectrometer was achieved by means of a specially constructed control system. A block diagram of the control system is shown in Fig. 1. Signals from the x-ray counter are sent to a single channel analyzer where an energy window is set around the x rays of interest. The output signals from the single-channel analyzer then go to the spectrometer control system from which they are sent to a multichannel analyzer operated in the external-time-base multiscale mode. Beam monitor signals are derived from a digital current integrator. The number of monitor counts desired at each spectrometer counting position is selectable by thumbwheel switches located on the front panel of the

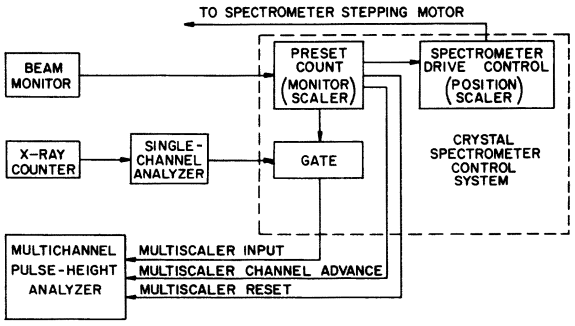

FIG. 1. Block diagram of the crystal-spectrometer control system.

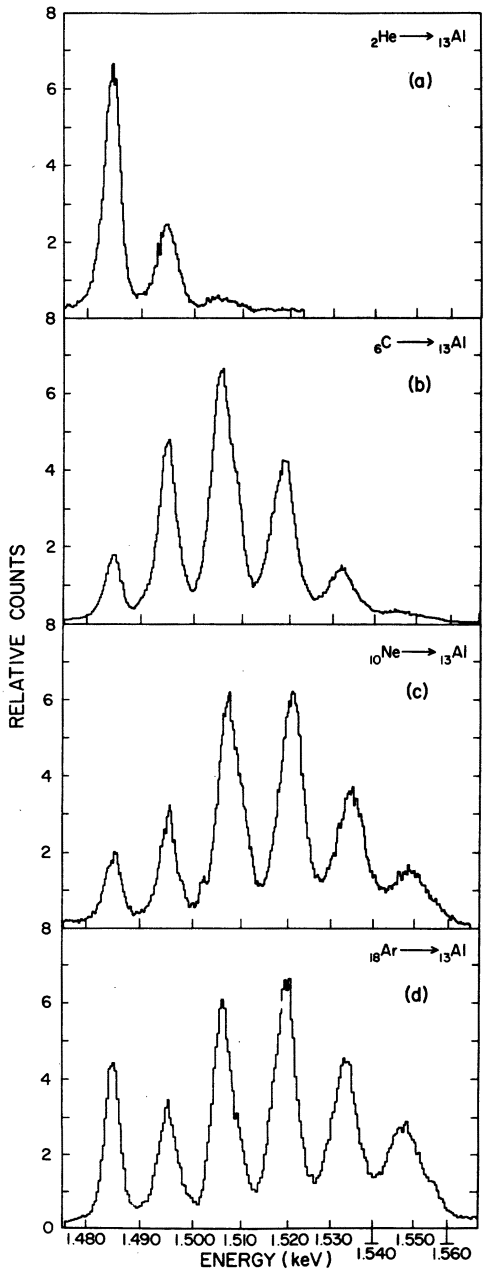

FIG. 2. Al $K\alpha$ x-ray spectra obtained with 1.7-MeV/amu He, C, Ne, and Ar ions.

control system. When the selected number of monitor counts has been collected, the system automatically steps the spectrometer to the next counting position and advances the multiscaler. The number of steps from one counting position to the next can be selected via another set of front-panel thumb-wheel switches. Both the number of monitor counts and the spectrometer counting position are displayed by arrays of light-emitting diodes located on the front panel of the control system. The complete control system occupies a double-width NIM module.

Typical $K\alpha$ x-ray spectra obtained with 1.7-MeV/amu He, C, Ne, and Ar ions are shown in Fig. 2 for Al, Fig. 3 for Cl, and Fig. 4 for K. In general, at least two spectra were taken for each projectile-target combination and in some cases as many as four spectra were obtained. Sufficient counts were

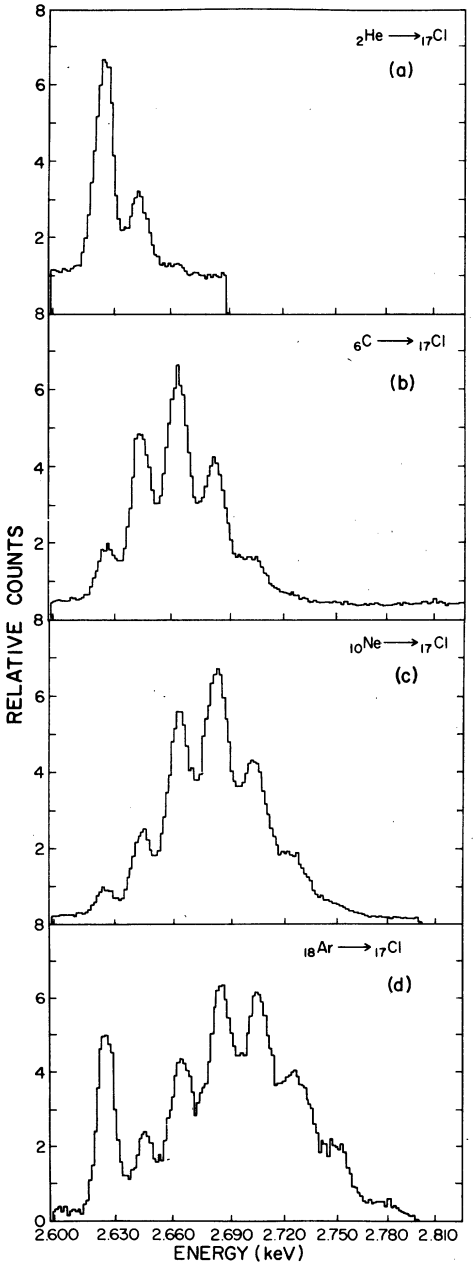

FIG. 3. Cl $K\alpha$ x-ray spectra obtained with 1.7-MeV/amu He, C, Ne, Ar ions.

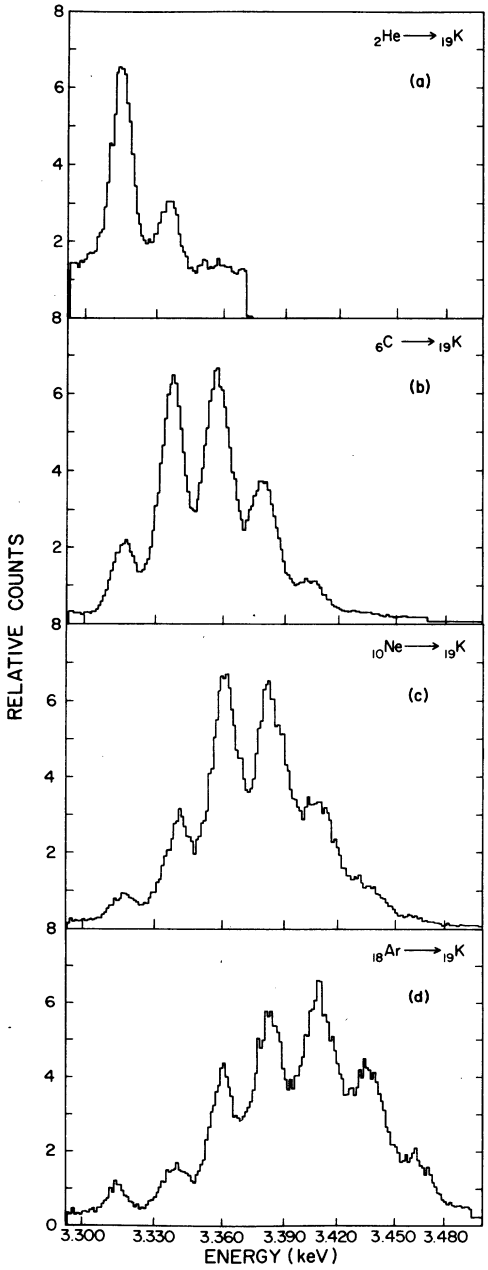

FIG. 4. K $K\alpha$ x-ray spectra obtained with 1.7-MeV/amu He, C, Ne, and Ar ions.

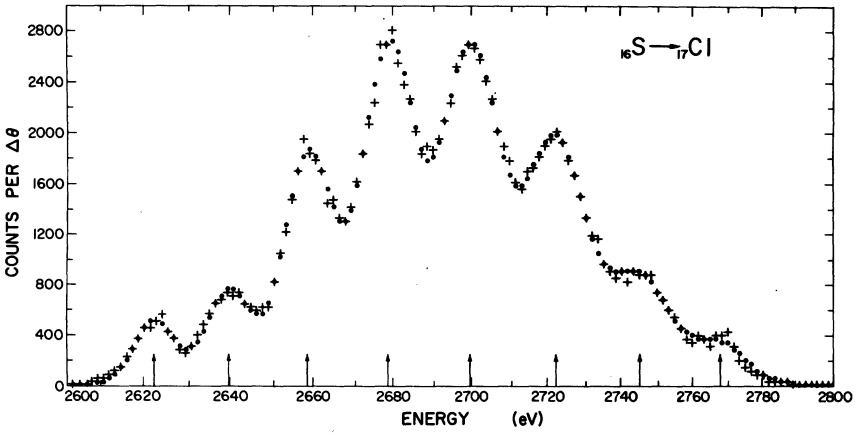

FIG. 5. Least-squares-fitted $K\alpha$ x-ray spectrum for 1.7-MeV/amu S ions incident on Cl. Crosses, data points; dots, calculated points. The arrows show the centroids of the fitted peaks.

usually accumulated such that the lowest intensity peaks were defined by statistical errors of less than 4%. Seven satellite peaks are discernible in the Cl and K spectra, whereas only five can be seen in the Al spectra due to the fact that the sixth and seventh satellite peaks are greatly attenuated by the Al K-absorption edge at 1559 eV.

III. ANALYSIS AND RESULTS

All of the spectra were analyzed by means of a least-squares peak fitting procedure (which has been described elsewhere[14]) to accurately determine the energies and relative intensities of the various $K\alpha$ peaks. An example of the quality of the fits typically obtained is shown in Fig. 5.

Absolute energies were assigned to each satellite peak by adding its measured relative energy with respect to the $K\alpha_{1,2}$ peak to the $K\alpha_{1,2}$ energies given by Bearden.[15] The $K\alpha$ satellite energies are listed in Tables I, II, and III. In the case of the Al satellites, no systematic variation of the peak energies with projectile atomic number could be discerned. The listed energies are the averages obtained for all runs with all projectiles and the indicated errors are root-mean-square deviations. In the Cl and K measurements, a linear increase in the peak energies was observed as a function of increasing projectile atomic number. Hence, in Tables II and III we have listed the satel-

TABLE I. $K\alpha$ x-ray energies for $_{13}$Al.

X-ray peak	Initial-state vacancy configuration	X-ray energy[a] (eV)	Energy difference (eV) Present work	Knudson *et al.*[b]	Hopkins *et al.*[c]	HFS calc.[d]
1	$1s^{-1}$	1486.6	0	0	0	0
2	$\{1s^{-1}2s^{-1}, 1s^{-1}2p^{-1}\}$	1496.9±0.1	10.3	10	10	$\{8, 10\}$ (10)
3	$\{1s^{-1}2s^{-2}, 1s^{-1}2s^{-1}2p^{-1}, 1s^{-1}2p^{-2}\}$	1507.9±0.2	21.3	21	21	$\{17, 19\,(20), 21\}$
4	$\{1s^{-1}2s^{-2}2p^{-1}, 1s^{-1}2s^{-1}2p^{-2}, 1s^{-1}2p^{-3}\}$	1521.3±0.3	34.7	35	33	$\{29, 32\,(33), 35\}$
5	$\{1s^{-1}2s^{-2}2p^{-2}, 1s^{-1}2s^{-1}2p^{-3}, 1s^{-1}2p^{-4}\}$	1535.1±0.3	48.5	48	46	$\{43, 46\,(46), 49\}$
6	$\{1s^{-1}2s^{-2}2p^{-3}, 1s^{-1}2s^{-1}2p^{-4}, 1s^{-1}2p^{-5}\}$	1549.9±0.5	63.3	62	59	$\{59, 63\,(62), 66\}$

[a] The $K\alpha_{1,2}$ energy (peak 1) was obtained from Ref. 15. The satellite energies were determined by adding this number to the measured $K\alpha_{1,2}$-satellite peak-energy separations.

[b] Reference 2.

[c] Reference 3.

[d] The numbers in parentheses are statistically weighted averages of the HFS energy differences for the various configurations.

lite energies for Ne-ion projectiles, and the number (in brackets) immediately following each measured satellite energy indicates the range of this energy variation for that particular peak in going from Ne- to He- or Ar-ion projectiles. That is, subtraction of this number from the listed satellite energy gives the satellite energy expected when He ions are the projectiles, whereas addition gives the satellite energy expected when Ar ions are the projectiles. The absolute errors in the satellite energies for Cl and K are essentially the same as those given for Al.

The $K\alpha$ x-ray relative intensities are listed in Table IV. These numbers have been corrected for the following effects:

(i) Absorption in the target. Uniform x-ray production throughout the target was assumed and mass absorption coefficients were taken from Storm and Israel.[16] The maximum satellite peak relative intensity change due to this correction was 1.9% for Al, 2.7% for Cl, and 7.8% for K.

(ii) Variation of crystal reflectivity with Bragg angle. This correction was determined experimentally for each Bragg crystal by comparing the relative intensities of K x rays emitted from targets containing several elements within the reflection range of the particular Bragg crystal, as determined directly from the proportional counter pulse-height spectrum at $2\theta = 0°$, with those determined from the Bragg reflection spectrum. The maximum satellite-peak relative intensity change due to this correction was 2.7% for Al, 12.5% for Cl, and 9.6% for K.

(iii) Absorption in the proportional counter window and proportional counter efficiency. These corrections were calculated from the known dimensions of the proportional counter and its window using mass absorption coefficients from Ref. 16. The maximum satellite-peak relative intensity change due to this correction was 2.2% for Al, 3.9% for Cl, and 0.1% for K.

In addition to the above corrections, it was necessary to correct the $K\alpha_{1,2}$ line intensities in the S+Al, Ar+Al, and Ar+Cl spectra for photoionization by projectile K x rays. Since for these combinations the projectile K x rays have energies greater than the target atom K-shell binding energies, K x-ray production as a result of photoionization can substantially alter the relative $K\alpha_{1,2}$ line intensities. This effect is demonstrated in Fig. 6, where a Cl $K\alpha$ x-ray spectrum for S ions incident on an NaCl target is compared with the spectrum obtained under the same conditions with a KCl target. In the case of S+NaCl, Cl K x-ray production by photoionization is not possible because the S K x-ray energy is smaller than the

TABLE II. $K\alpha$ x-ray energies for $_{17}$Cl.

X-ray peak	Initial-state vacancy configuration	X-ray energy[a] (eV)	Energy difference (eV) Present work	Energy difference (eV) HFS calc.[b]
1	$1s^{-1}$	2621.9	0	0
2	$1s^{-1}2s^{-1}$, $1s^{-1}2p^{-1}$	2640.2[±1.4]	18.3	11, 15 (14)
3	$1s^{-1}2s^{-2}$, $1s^{-1}2s^{-1}2p^{-1}$, $1s^{-1}2p^{-2}$	2658.8[±1.8]	36.9	24, 28 (30), 32
4	$1s^{-1}2s^{-2}2p^{-1}$, $1s^{-1}2s^{-1}2p^{-2}$, $1s^{-1}2p^{-3}$	2678.5[±2.2]	56.6	42, 46 (47), 50
5	$1s^{-1}2s^{-2}2p^{-2}$, $1s^{-1}2s^{-1}2p^{-3}$, $1s^{-1}2p^{-4}$	2699.1[±2.0]	77.2	61, 66 (66), 70
6	$1s^{-1}2s^{-2}2p^{-3}$, $1s^{-1}2s^{-1}2p^{-4}$, $1s^{-1}2p^{-5}$	2720.3[±2.8]	98.4	81, 87 (85), 92
7	$1s^{-1}2s^{-2}2p^{-4}$, $1s^{-1}2s^{-1}2p^{-5}$	2743.5[±2.7]	121.6	105, 111 (108)
8	$1s^{-1}2s^{-2}2p^{-5}$	2769.8[±3.6]	147.9	131

[a] The $K\alpha_{1,2}$ energy (peak 1) was obtained from Ref. 15. The satellite energies were determined by adding this number to the measured $K\alpha_{1,2}$-satellite peak-energy separations. The listed energies are those obtained with Ne ions and the numbers in square brackets indicate the extent to which the peak energy is expected to vary in going from He-ion to Ar-ion projectiles.

[b] The numbers in parentheses are statistically weighted averages of the HFS energy differences for the various configurations.

TABLE III. $K\alpha$ x-ray energies for $_{19}$K.

X-ray peak	Initial-state vacancy configuration	X-ray energy[a] (eV)	Energy difference (eV) Present work	Energy difference (eV) HFS calc.[b]
1	$1s^{-1}$	3312.9	0	0
2	$1s^{-1}2s^{-1}$, $1s^{-1}2p^{-1}$	3336.0[±3.2]	23.1	14, 18 (17)
3	$1s^{-1}2s^{-2}$, $1s^{-1}2s^{-1}2p^{-1}$, $1s^{-1}2p^{-2}$	3357.1[±4.0]	44.2	28, 33 (36), 38
4	$1s^{-1}2s^{-2}2p^{-1}$, $1s^{-1}2s^{-1}2p^{-2}$, $1s^{-1}2p^{-3}$	3379.1[±4.7]	66.2	49, 54 (55), 59
5	$1s^{-1}2s^{-2}2p^{-2}$, $1s^{-1}2s^{-1}2p^{-3}$, $1s^{-1}2p^{-4}$	3402.3[±5.7]	89.4	71, 76 (76), 82
6	$1s^{-1}2s^{-2}2p^{-3}$, $1s^{-1}2s^{-1}2p^{-4}$, $1s^{-1}2p^{-5}$	3427.5[±5.2]	114.6	95, 101 (100), 107
7	$1s^{-1}2s^{-2}2p^{-4}$, $1s^{-1}2s^{-1}2p^{-5}$	3452.7[±5.6]	139.8	121, 127 (124)
8	$1s^{-1}2s^{-2}2p^{-5}$	3481.2[±5.6]	168.3	150

[a] The $K\alpha_{1,2}$ energy (peak 1) was obtained from Ref. 15. The satellite energies were determined by adding this number to the measured $K\alpha_{1,2}$-satellite peak-energy separations. The listed energies are those obtained with Ne ions and the numbers in square brackets indicate the extent to which the peak energy is expected to vary in going from He-ion to Ar-ion projectiles.

[b] The numbers in parentheses are statistically weighted averages of the HFS energy differences for the various configurations.

TABLE IV. Relative $K\alpha$ x-ray satellite intensities for Al, Cl, and K using 1.7-MeV/amu projectiles.

Target projectile		Number of L-shell vacancies							
		0	1	2	3	4	5	6	7
$_{13}$Al	$_{1}$H	0.858	0.142						
	$_{2}$He	0.664	0.285	0.051					
	$_{6}$C	0.068	0.215	0.366	0.239	0.090	0.023		
	$_{8}$O	0.045	0.128	0.312	0.293	0.168	0.053		
	$_{10}$Ne	0.053	0.101	0.276	0.294	0.192	0.085		
	$_{16}$S	0.123	0.094	0.218	0.233	0.202	0.130		
	$_{18}$Ar	0.128	0.094	0.220	0.247	0.176	0.135		
$_{17}$Cl	$_{2}$He	0.680	0.320						
	$_{6}$C	0.053	0.229	0.363	0.256	0.094	0.005		
	$_{8}$O	0.028	0.133	0.304	0.316	0.170	0.049		
	$_{10}$Ne	0.018	0.080	0.232	0.330	0.224	0.097	0.018	
	$_{16}$S	0.026	0.046	0.136	0.229	0.244	0.205	0.091	0.023
	$_{18}$Ar	0.038	0.061	0.142	0.232	0.236	0.179	0.095	0.018
$_{19}$K	$_{2}$He	0.765	0.235						
	$_{6}$C	0.074	0.307	0.353	0.208	0.058			
	$_{8}$O	0.045	0.185	0.316	0.271	0.142	0.042		
	$_{10}$Ne	0.022	0.113	0.299	0.303	0.184	0.070	0.009	
	$_{16}$S	0.019	0.061	0.176	0.261	0.262	0.175	0.047	
	$_{18}$Ar	0.021	0.046	0.147	0.227	0.266	0.208	0.075	0.010

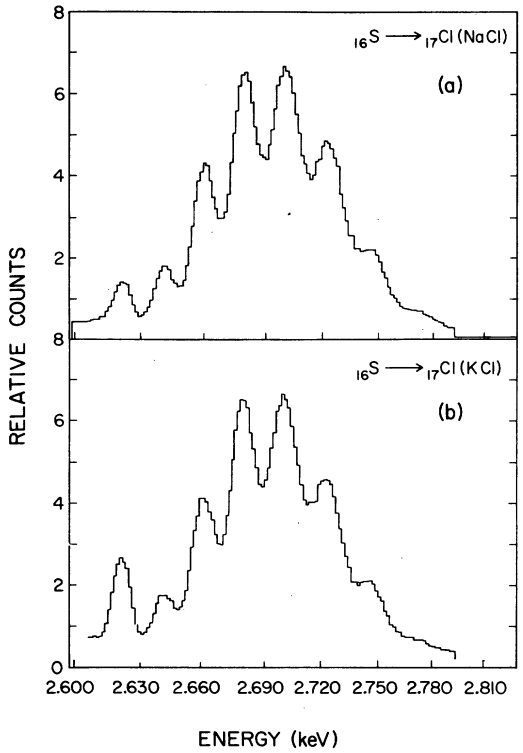

FIG. 6. (a) Cl $K\alpha$ x-ray spectrum for 1.7-MeV/amu S ions incident on a NaCl target. (b) Cl $K\alpha$ x-ray spectrum for 1.7-MeV/amu S ions incident on a KCl target. The $K\alpha_{1,2}$ peak is enhanced due to Cl K-shell photoionization by K K x-rays.

Cl K-shell binding energy and a typical binomial satellite intensity pattern is observed. In the case of S + KCl, however, Cl K x-ray production by photoionization is possible via the K K x rays generated as a result of S + K collisions. Here (Fig. 6b) it is seen that the Cl $K\alpha_{1,2}$ peak is considerably enhanced because of this effect. Only the $K\alpha_{1,2}$ peak is affected because photoionization does not cause appreciable amounts of multiple ionization.

In order to correct for this effect, it was necessary to measure the relative yields of target and projectile K x rays. This was done using a Si(Li) x-ray spectrometer system giving an energy resolution of 230 eV (FWHM) at 6.4 keV. The efficiency of this system was carefully determined from 3.3 to 59.5 keV by means of calibrated sources as described in Ref. 17 and it was extended down to 1.4 keV using the semiempirical method discussed in Ref. 18. From the measured projectile-to-target K x-ray yield ratio, the relative $K\alpha_{1,2}$ peak enhancement could be predicted from the relationship

$$\frac{I_{\text{phot}}}{I_{\text{tot}}} = \frac{Y_P(\epsilon_T T_T)}{Y_T(\epsilon_P T_P)}\omega_T(1-T), \tag{1}$$

where Y_P/Y_T is the measured projectile-to-target K x-ray yield ratio; ϵ_P, ϵ_T are the detection efficiencies for projectile and target K x rays; T_P, T_T are the transmission factors accounting for absorption of projectile and target K x rays in

the target; ω_T is the normal K-shell fluorescence yield for the target atoms; and $1-T$ is the fraction of projectile K x rays which undergo target-atom K-electron photoionization in the target.

In applying the above equation it was assumed that both projectile and target x rays were produced uniformly throughout the target and the fluorescence yields given by Bambynek *et al.*[19] were used. The required mass absorption coefficients and K-shell photoionization cross sections were taken from Ref. 16.

As a check of the accuracy with which the photoionization correction could be determined, measurements were also performed for O+NaCl and O+KCl, as well as for S+NaCl and S+KCl. The results of these experiments are summarized in Table V. Listed in the first column of Table V is the $K\alpha_{1,2}$ peak intensity enhancements observed in the Bragg spectrometer measurements. In the first two cases (O+NaCl/KCl and S+NaCl/KCl), these numbers are the differences between the Cl $K\alpha_{1,2}$ relative intensities obtained with KCl targets and those obtained with the NaCl targets. The numbers for Ar+NaCl, S+Al, and Ar+Al are the differences between the measured Cl and Al $K\alpha_{1,2}$ relative intensities and those predicted from binomial fits to the various satellite peak intensities. In cases where photoionization enhancement of the $K\alpha_{1,2}$ peak is not possible, deviations between measured $K\alpha_{1,2}$ peak intensities and those given by binomial fits to the satellite intensities are typically of the order of 20%. We have therefore used this as an estimate of the error in the listed enhancements for these cases. The second column contains the $K\alpha_{1,2}$ peak-intensity enhancements expected due to photoionization as determined from the Si(Li) relative-intensity measurements. The rather large errors associated with the Al measurements result from the uncertainty in the relative detection efficiency for Al K x rays with the Si(Li) system. Additional checks were performed with a flow proportional counter, however, and the same results were obtained.

It is seen in Table V that the measured photoionization contributions for O+NaCl/KCl and S+NaCl/KCl are in very good agreement with the $K\alpha_{1,2}$ enhancements observed in the crystal-spectrometer measurements. We are therefore confident that our Si(Li) measurements give accurate determinations of the intensity contribution from photoionization. In the case of Ar+NaCl it is seen that most of the $K\alpha_{1,2}$ enhancement is accounted for by photoionization, but in the cases of S+Al and Ar+Al, photoionization accounts for only a small fraction of the observed $K\alpha_{1,2}$ enhancement. The Al $K\alpha_{1,2}$ peak intensity obtained with S ions is a factor of 6.7 larger than expected on the basis of a binomial fit to the satellite intensities and only 9% of this discrepancy is attributable to photoionization of Al atoms by S K x rays. The Al $K\alpha_{1,2}$ peak intensity obtained with Ar ions is a factor of 6.0 larger than expected on the basis of a binomial fit to the satellite intensities and only 4% of this discrepancy is attributable to photoionization of Al atoms by Ar K x rays. We have also fit binomial distributions to the relative intensities given by Hopkins *et al.*[3] for 0.73 to 1 MeV/amu Cl ions incident on Al and find that *both* the $K\alpha_{1,2}$ peak and the first satellite peak appear to be enhanced in these spectra. A similar effect has recently been noted by Knudson, Burkhalter, and Nagel in $K\alpha$ x-ray spectra of Mg, Al, and Si obtained with 0.08 to 0.1 MeV/amu Ar ions.[20]

TABLE V. Comparison of the observed $K\alpha_{1,2}$ intensity enhancements with the intensity contributions expected from photoionization.

Projectile/Target	$\Delta I_{(K\alpha_{1,2})}$ (×100)	$I_{\text{phot.}}$ (×100)
O+NaCl/KCl	1.5±0.2	1.9±0.3(K→ Cl)
S+NaCl/KCl	2.4±0.3	2.3±0.4(K→ Cl)
Ar+NaCl	9.9±2.0	7.2±1.0(Ar→ Cl)
S+Al	11.2±2.2	1.0±0.3(S→ Al)
Ar+Al	11.5±2.3	0.5±0.2(Ar→ Al)

As has already been mentioned, previous investigators have found that the $K\alpha$ x-ray spectra resulting from ion-atom collisions could be well represented by binomial distributions. Specifically, it is found that the relative intensity of each $K\alpha$ peak is closely given by the nth term of a binomial series

$$\frac{I_n}{I_{\text{tot}}} \simeq \binom{n_L}{n} \bar{p}_L^{\,n}(1-\bar{p}_L)^{n_L-n}, \tag{2}$$

where

$$\binom{n_L}{n} = n_L!/(n_L-n)!n!$$

in which n_L is the number of L-shell electrons in the ground state, n is the number of L-shell vacancies associated with the particular $K\alpha$ peak under consideration, and $\bar{p}_L$ is a binomial probability parameter. In the event that L-shell vacancy transfer transitions do not seriously compete with $K\alpha$ x-ray emission, the parameter $\bar{p}_L$ may be interpreted as being the average L-shell ionization probability *per electron* for K-shell ionizing collisions and the meaning of Eq. (2) is straightforward; $\bar{p}_L^{\,n}$ is the probability of ionizing n L-shell electrons and $(1-\bar{p}_L)^{n_L-n}$ is the prob-

ability of not ionizing any of the rest. The binomial coefficient $\binom{n_L}{n}$ is the number of different ways of ionizing n out of n_L electrons.

Using a least-squares binomial-distribution fitting procedure the best value of $\bar{p}_L$ was determined for each of the measured $K\alpha$ spectra. Examples of these fits are shown in Fig. 7 for He, C, O, and Ne ions incident on Al. The shaded rectangles show the measured relative intensities of the various satellite lines (n is the number of L-shell vacancies) and the open rectangles show the intensities given by Eq. (2) using the $\bar{p}_L$ value listed in the figure. In general, the fits are quite good with the average deviations between measured and calculated intensities being about 18% in the worst cases. Similar results were obtained for Cl and K.

The $K\alpha$ x-ray intensities for S and Ar incident on Al were fitted on the assumption that two independent mechanisms contribute to the generation of the observed spectra. These anomalous spectra were reconstructed from a composite of two binomial distributions. Three parameters are required for this formulation; namely $\bar{p}_L^a$—the binomial probability parameter for mechanism a (which is presumably the same mechanism as pertains to the H, He, C, O, and Ne ion results); $\bar{p}_L^b$—the binomial probability parameter for mechanism b; and f_b—the fraction of the total x-ray yield due to mechanism b. Representing the relative intensity of a particular satellite peak corresponding to n L-shell vacancies by P_{KL_n}, we may write

$$P_{KL_n} = f_b P^b_{KL_n} + (1 - f_b) P^a_{KL_n} . \tag{3}$$

where $P^a_{KL_n}$ and $P^b_{KL_n}$ are obtained from Eq. (2) using $\bar{p}_L^a$ and $\bar{p}_L^b$, respectively. We first of all note that if $\bar{p}_L^a = \bar{p}_L^b$, then $P^a_{KL_n} = P^b_{KL_n}$, and therefore $P_{KL_n} = P^a_{KL_n}$, in which case the $K\alpha$ intensity distribution would not reflect the presence of an additional mechanism for $K\alpha$ x-ray production. It is readily apparent that $\bar{p}_L^b$ has to be much smaller than $\bar{p}_L^a$ to produce the kind of intensity patterns displayed by the S + Al and Ar + Al spectra. In Fig. 8 are shown fits to the Ar + Al $K\alpha$ x-ray intensities using two different sets of parameters. As can be seen from this figure, the best fits are obtained with $\bar{p}_L^b$ near or equal to zero.

Listed in Table VI are the $\bar{p}_L$ values obtained from binomial fits to the Al, Cl, and K $K\alpha$ x-ray spectra, as described above. In the cases of S + Al and Ar + Al, the fits were made assuming $\bar{p}_L^b = 0$. The error bars assigned to the $\bar{p}_L$ values

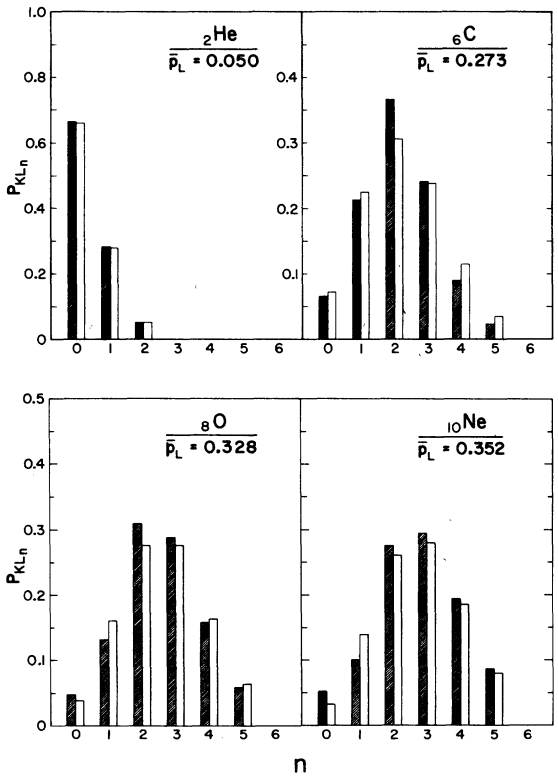

FIG. 7. Binomial fits to the Al $K\alpha$ x-ray relative intensities obtained with 1.7-MeV/amu He, C, O, and Ne ions. Shaded rectangles, measured relative intensities; open rectangles, relative intensities calculated from Eq. (2) using the indicated value of $\bar{p}_L$. (n is the number of L-shell vacancies which specifies each peak.)

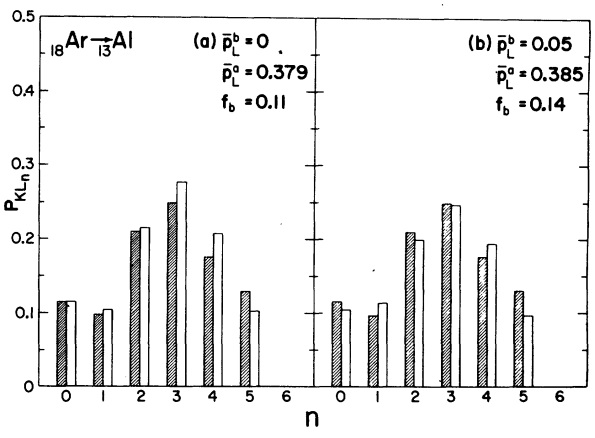

FIG. 8. Reconstruction of the measured Al $K\alpha$ x-ray relative intensities obtained with 1.7-MeV/amu Ar ions (shaded rectangles) by a composite of two binomial distributions (open rectangles) using (a) $\bar{p}_L^b = 0$ and (b) $\bar{p}_L^b = 0.05$. The listed values of $\bar{p}_L^a$ and f_b are those leading to the best representations of the measured relative intensities.

are the root-mean-square deviations obtained in fits to two or more spectra.

IV. DISCUSSION

A. X-ray energies

In Tables I, II, and III the measured $K\alpha$ x-ray satellite energy differences (relative to the $K\alpha_{1,2}$ line) are compared with the results of Hartree-Fock-Slater (HFS) calculations for the various possible L-shell vacancy configurations. The HFS x-ray energies were obtained by taking the differences between total energies for the appropriate initial and final states as calculated using the program of Herman and Skillman[21] with unmodified Slater exchange. It is apparent that only one L-shell vacancy configuration can contribute to peaks 1 and 8, whereas two can contribute to peaks 2 and 7, and three to peaks 3, 4, 5, and 6. The predicted energy differences between adjacent configurations for a given number of L-shell vacancies ranges from 2 to 3 eV for Al and from 4 to 6 eV for Cl and K. A number of different $K\alpha$ x-ray transition lines will of course be associated with each L-shell vacancy configuration as a result of LS coupling between the incompletely filled subshells. For example, in the case of single K- plus single L-shell ionization, two initial states (^1S, ^3S) for the vacancy configuration $1s^{-1}2s^{-1}$ and two initial states (^1P, ^3P) for the vacancy configuration $1s^{-1}2p^{-1}$ are possible. The $1s^{-1}2s^{-1}$ states can decay by $K\alpha$ transitions to ^1P and ^3P final states, respectively, while the $1s^{-1}2p^{-1}$ states can decay by $K\alpha$ transitions to ^1S or ^1D, and ^3P final states, respectively.[22,23] Thus the second peak appearing in each of the $K\alpha$ spectra shown in Figs. 2–4 contains possible contributions from five x-ray lines. Indeed, evidence of complex structure is readily apparent in the Al spectra (Fig. 2) where the average 2θ widths (FWHM) change from 0.85° to 0.99°, 1.2°, 1.3°, 1.5°, and 1.6° in going from peak 1 to peak 2, 3, 4, 5, and 6, respectively. In addition, some of the x-ray peak shapes are seen to be quite asymmetric.

TABLE VI. Experimental and theoretical values of the binomial probability parameter $\bar{p}_L$ for Al, Cl, and K $K\alpha$ x-ray satellite production by 1.7-MeV/amu projectiles.

Target	Projectile	Experiment $\bar{p}_L$	Theory $\bar{p}_{2s}$	Theory $\bar{p}_{2p}$	Theory $\bar{p}_L$
$_{13}$Al	$_1$H	0.019±0.002	0.070	0.178	0.142
	$_2$He	0.050±0.002	0.244	0.542	0.423
	$_6$C	0.273±0.003	0.838	0.998	0.945
	$_8$O	0.328±0.003	0.900	1.000	0.967
	$_{10}$Ne	0.352±0.005	0.978	1.000	0.993
	$_{16}$S	0.388±0.005	1.000	1.000	1.000
	$_{18}$Ar	0.379±0.005	1.000	1.000	1.000
$_{17}$Cl	$_2$He	0.050±0.003	0.099	0.249	0.199
	$_6$C	0.275±0.003	0.581	0.913	0.802
	$_8$O	0.335±0.005	0.768	0.986	0.913
	$_{10}$Ne	0.382±0.005	0.882	0.999	0.960
	$_{16}$S	0.479±0.005	0.990	1.000	0.997
	$_{18}$Ar	0.463±0.005	0.996	1.000	0.999
$_{19}$K	$_2$He	0.034±0.002	0.070	0.155	0.127
	$_6$C	0.236±0.002	0.465	0.781	0.676
	$_8$O	0.305±0.003	0.660	0.932	0.841
	$_{10}$Ne	0.341±0.005	0.802	0.985	0.924
	$_{16}$S	0.442±0.005	0.974	1.000	0.991
	$_{18}$Ar	0.478±0.005	0.988	1.000	0.996

The numbers enclosed by parentheses in the HFS columns of Tables I, II, and III are statistically weighted averages of the energy differences calculated for all the various L-shell vacancy configurations contributing to a given peak. The statistical weighting factors used take into account only the statistical probability of forming a particular L-shell vacancy configuration given that a total of n equivalent L-shell electrons are ejected and neither account for differences in the ionization cross sections of $2s$ and $2p$ electrons, nor for $2s$ vacancy disappearance via Coster-Kronig transitions. Nevertheless the calculated average energy differences would not be expected to change by more than about 4 eV even if these effects could be taken into account and hence they provide useful numbers for comparison with the experimental energy differences.

It is seen in Table I that the HFS average energy differences for Al agree quite well with the experimental measurements. The HFS average energy differences listed in Tables II and III for Cl and K, however, are systematically smaller than the experimental values. An interesting trend is discerned when the experimental and HFS $K\alpha$ x-ray energy differences are plotted as a function of atomic number, as in Fig. 9. In this figure, the solid lines connect data points for satellite lines corresponding to a particular number of L-shell vacancies (n). The solid data points for Si and Mg are from the measurements of McCrary *et al.*[5,6] The dashed lines show the average HFS x-ray energy differences calculated as described above. As can be seen in this figure, the deviations between the measured and calculated energy differences increase monotonically both with increasing target atomic number and with increasing number of L-shell vacancies.

Similar deviations between measured and (HFS) calculated satellite energy differences have been observed by Jundt and Nagel.[24] These investigators find much better agreement with Hartree-Fock calculations and therefore conclude that the inability of the HFS calculations to accurately reproduce the experimental energy differences is directly attributable to the Slater exchange ap-

proximation.[25] Unfortunately, one is prevented from making a detailed assessment of the magnitude of this effect because the exact amount of outer-shell ionization present at the time of $K\alpha$ x-ray emission is unknown. The effect of outer-shell ionization on the HFS x-ray energy differences is illustrated for Cl in Fig. 10. In this figure, the average HFS $K\alpha$ x-ray energy differences for each satellite peak (solid circles) are plotted as a function of the number of M-shell vacancies. The horizontal bands indicate the ranges of the experimentally observed energy differences. It is apparent from this figure that four to seven M-shell vacancies would be required to fully account for the measured energy differences in terms of outer-shell ionization alone. The results of a recent study of $K\beta/K\alpha$ intensity ratios for carbon-ion induced x-ray emission,[17] however, suggest that the average amount of M-shell ionization is less than this. On the other hand, variation of the amount of M-shell ionization is quite likely the cause of the satellite peak energy and width changes with increasing projectile atomic number.

B. X-ray intensities

The dependence of the binomial probability parameter $\bar{p}_L$ on projectile atomic number (Z_1) is shown in Fig. 11. In general, the curves rise quite rapidly with increasing projectile atomic number, reach a maximum near $Z_1 = Z_2$ and begin to decrease at high-projectile atomic numbers. An interesting feature is the significant rise in the Cl and K $\bar{p}_L$ values above those for Al for $Z_1 \gtrsim 10$. This is in direct opposition to the behavior expected on the basis of the L-shell ionization cross section for Coulomb excitation. Estimates using the binary-encounter model[26] indicate that the L-shell ionization cross section for Al is roughly three times larger than that for Cl and five times larger than that for K. Of course vacancy-transfer effects will tend to decrease the measured $\bar{p}_L$ values from those which truly characterize the ionization distribution, but as we shall show later, these effects would be expected to be less important for Al than for Cl

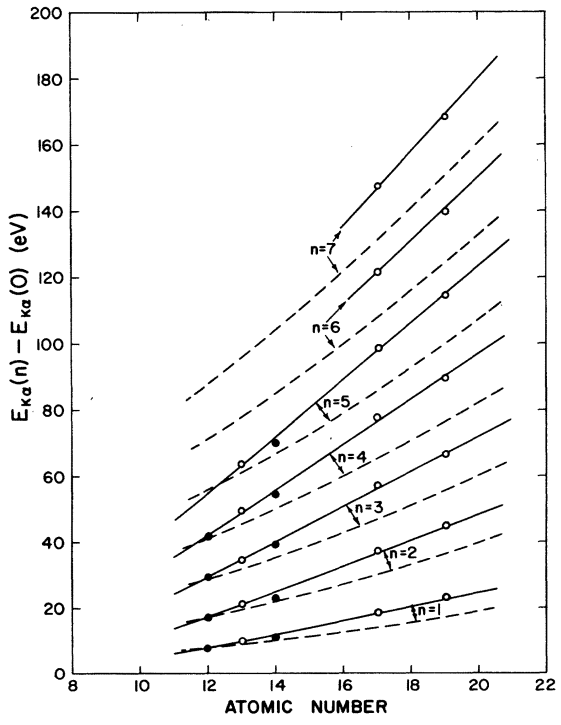

FIG. 9. Comparison of the measured $K\alpha_{1,2}$-$K\alpha$ satellite energy differences (data points) with those calculated using the HFS program of Herman and Skillman (Ref. 21) (dashed curve). n is the number of L-shell vacancies which specifies each satellite peak. The solid data points for Si and Mg are from Refs. 5 and 6, respectively.

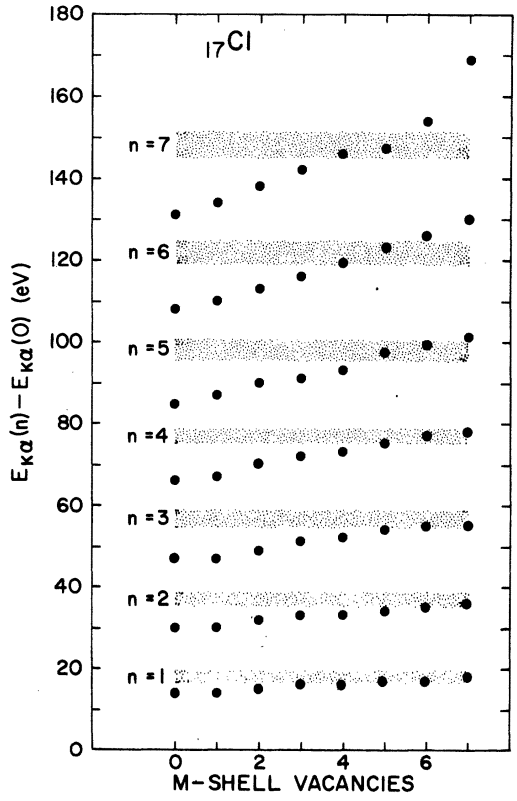

FIG. 10. Calculated (HFS) effect of M-shell vacancies on the $K\alpha_{1,2}$-$K\alpha$ satellite energy differences for Cl (dots). n is the number of L-shell vacancies which specifies each satellite peak. The shaded bands indicate the ranges of the experimentally observed energy differences.

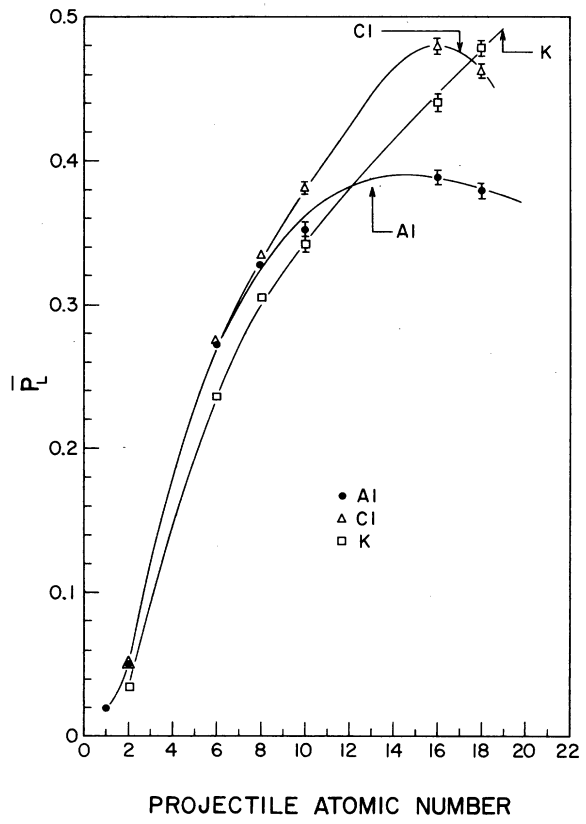

FIG. 11. Binomial probability parameters $\bar{p}_L$ for 1.7-MeV/amu projectiles incident on Al, Cl, and K as a function of projectile atomic number. The arrows indicate the locations of symmetric ($Z_1 = Z_2$) projectile-target combinations.

and K. The above mentioned behavior, and in particular the apparent maximization of $\bar{p}_L$ when projectile and target atomic numbers are nearly the same, indicates that level matching effects exert a considerable influence on the multiple L-shell ionization process.

In attempting to compare the projectile and target atomic-number dependences of our data with those expected for a direct Coulomb-excitation mechanism, we have employed an impact-parameter formulation of the binary-encounter approximation (BEA) as developed by Hansen.[27] The reasons for adopting this approach are (i) that the BEA results have been found to closely reproduce the excitation functions for K-shell ionization by α particles over a wide range of projectile velocities and target atomic numbers,[28] and (ii) that calculations of $\bar{p}_L$ are relatively easy to carry out within the framework of this model. The impact-parameter dependence of the K-shell ionization probability as given by Hansen's calculations has been compared with the experimental data of Laegsgaard *et al.*[29] for 2-MeV protons incident on Se and the two are in excellent agreement.[27]

Using the Hansen formulation of the BEA we have calculated theoretical $\bar{p}_L$ values by taking a weighted average of the L-shell ionization probability *per electron* as a function of impact parameter $p_L(b)$ over impact parameter using the K-shell ionization cross section as the weighting factor:

$$\bar{p}_L = \int_0^\infty p_L(b) p_K(b) b\, db \Big/ \int_0^\infty p_K(b) b\, db . \qquad (4)$$

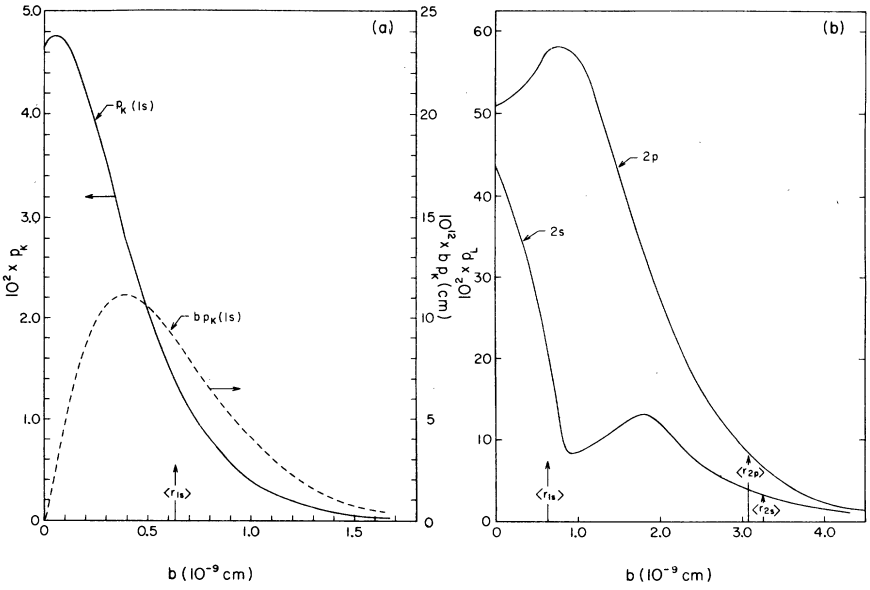

FIG. 12. Theoretical ionization probability curves for K- and L-shell ionization of Al by 1.7-MeV/amu He ions. The calculated ionization probabilities are based upon the impact-parameter formulation of the binary-encounter model by Hansen (Ref. 27).

The theoretical K- and L-shell ionization probabilities per electron for 1.7 MeV/amu He ions incident on Al are shown in Fig. 12. With regard to the L-shell ionization probability, it is seen that only the relatively small region inside the average K-shell radius $\langle r_K \rangle$ is of importance in K-shell ionizing collisions.

The theoretical $\bar{p}_L$ values calculated for all the various projectiles and targets used in the present work are presented in Table VI. One sees that the theoretical values are all much larger than the experimental values. Whereas the conditions for the validity of the BEA are not well met for the heavy-ion ($Z_1 > 2$) projectiles, it is surprising to find such large discrepancies between the theoretical and experimental $\bar{p}_L$ values for the H and He ions in view of the generally good agreement which has been found in total ionization cross section and K-shell ionization probability comparisons.

The dependence of $\bar{p}_L$ on target atomic number is shown in Fig. 13 for He and C ion projectiles. The data points denoted by the open circles were measured earlier by Li[30] employing a critical absorption technique.[9] The solid curves indicate the $\bar{p}_L$ values given by the BEA calculations. This figure graphically illustrates the large disparities noted above, but in addition shows that the experimental and theoretical $\bar{p}_L$ values converge as the target atomic number increases. The dashed curve in Fig. 13(b) was obtained by multiplying the dashed curve in Fig. 13(a) (which has been fitted to the data points) by the scaling factor $Z_C^2/Z_{He}^2 = 9$. It is apparent from this comparison that the experimental $\bar{p}_L$ values do not follow a Z_1^2 scaling law.

We shall now consider the effects of L-vacancy disappearance prior to $K\alpha$ x-ray emission. The consequences of competition between K- and L-vacancy filling processes can be schematically outlined as follows:

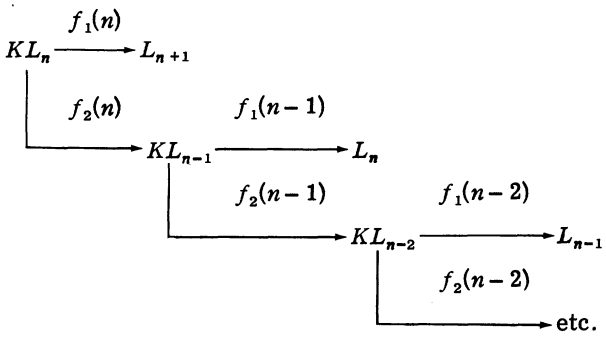

Start with a given number of initial configurations consisting of one K-shell vacancy and n L-shell vacancies and suppose the fraction $f_1(n)$ decays directly by $K\alpha$ x-ray emission and the fraction $f_2(n)$ transforms to configurations consisting of one K-shell vacancy and $(n-1)$ L-shell vacancies

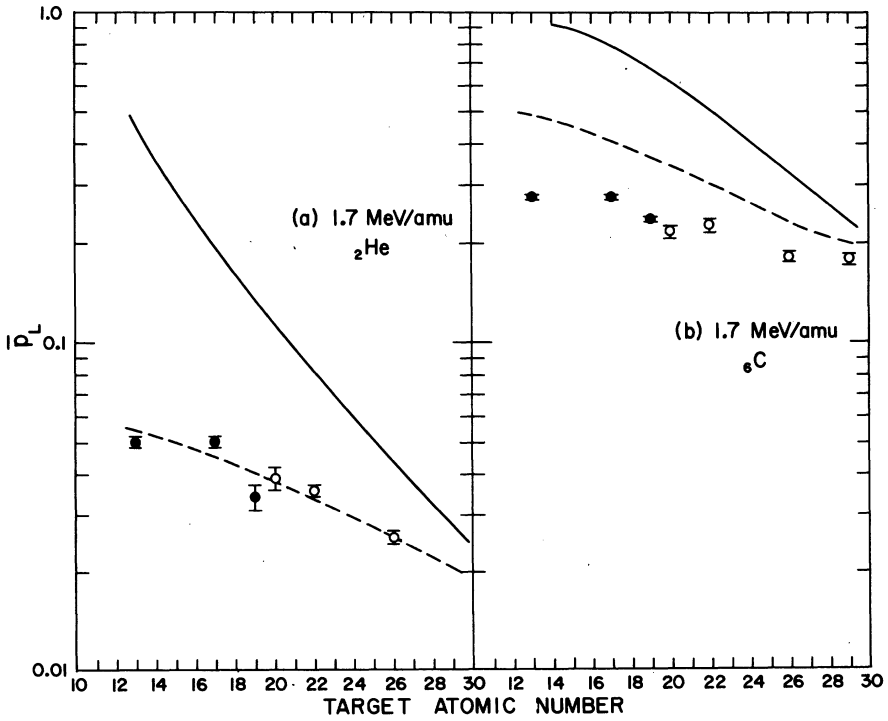

FIG. 13. Dependence of the binomial probability parameter $\bar{p}_L$ on target atomic number for 1.7-MeV/amu He and C ions. The open data points are from Ref. 30. The solid curves show the results of the BEA calculations. The dashed curve in (a) has been fit through the data points, while the dashed curve in (b) is this same curve multiplied by the scale factor $Z_C^2/Z_{He}^2 = 9$.

via transitions to the L-shell. Then let the fraction $f_1(n-1)$ of these configurations decay directly by $K\alpha$ x-ray emission and the fraction $f_2(n-1)$ transform to configurations consisting of one K-shell vacancy and $(n-2)$ L-shell vacancies... and so on. The fraction f_1 is the ratio of the $K\alpha$ width to the sum of the K- and L-shell widths, and the fraction f_2 is $\Gamma_L/(\Gamma_K+\Gamma_L)$. Hence, the number of $K\alpha$ x rays arising from a configuration having one K- and n L-shell vacancies depends not only on the number of such configurations formed initially, but also on the number of higher-order configurations which are produced as well. The relationship between the number of $K\alpha$ x rays emitted in the presence of n L-shell vacancies $N^{\alpha}_{KL_n}$ and the number of configurations consisting of one K- plus n L-shell vacancies originally formed in the collision process $N^{0}_{KL_n}$ is thus given by

$$N^{\alpha}_{KL_n} = f_1(n)[N^{0}_{KL_n} + f_2(n+1)N^{0}_{KL_{n+1}} + f_2(n+1)f_2(n+2)N^{0}_{KL_{n+2}} + \cdots] \quad (5)$$

or

$$N^{0}_{KL_n} = \frac{1}{f_1(n)}N^{\alpha}_{KL_n} - \frac{f_2(n+1)}{f_1(n+1)}N^{\alpha}_{KL_{n+1}}. \quad (6)$$

Unfortunately there have been no theoretical calculations or experimental measurements of K- and L-shell transition rates in atoms having single K- plus multiple L-shell vacancies and even if reasonable estimates of these rates could be made, our lack of knowledge concerning the configuration of the M shell would still make it impossible to apply the appropriate corrections with any certainty. In the case of the light-ion results, where the probability for multiple L-shell ionization is small, one can make an estimate of the effect of vacancy transfer on the experimental $\bar{p}_L$ values by neglecting changes of f_1 and f_2 with n and using transition widths for single K-shell and single L-shell vacancy states. We have computed the factors f_1 and f_2 for the elements Al through Ca and they are listed in Table VII. The $K\alpha$ widths are those given by Scofield[31]; the total K-shell widths were obtained by dividing Scofield's radiative widths by the K-shell fluorescence yields given by Bambynek *et al.*,[19] and the total L-shell widths are those given by McGuire.[32] When the He-ion results are corrected for L-vacancy transfer in this approximate way the $\bar{p}_L$ values for Al, Cl, and K are increased by 2%, 11%, and 16%, respectively. Hence, it is apparent that the conclusions reached above, resulting from comparisons of the experimental results for He ions with the BEA predictions, are not significantly changed by L-vacancy transfer considerations.

C. Al $K\alpha_{1,2}$ intensity enhancement

In Sec. III we noted a large enhancement of the Al $K\alpha_{1,2}$ peaks appearing in the spectra obtained with S and Ar ions and conjectured the cause of this effect to be a new mechanism for producing K-shell vacancies. We here consider the following as possible explanations for the $K\alpha_{1,2}$ intensity enhancements:

1. *K-vacancy production by projectile electrons.* It is well known that K-shell ionization by electrons does not result in large amounts of simultaneous L-vacancy production. Since the incident projectiles carry 13 of their own orbital electrons into the target in the case of Ar ions, it is conceivable that the $K\alpha_{1,2}$ intensity enhancement is caused by projectile-electron–induced ionization. We have rejected this mechanism for two reasons: (i) The K-shell ionization cross sections for electrons are too small to account for the observed intensity enhancements. Estimates based upon the work of Arthurs and Moiseiwitsch[33] indicate that the maximum cross section for K-shell ionization of Al by electrons is only about 0.1% of the cross section for K-shell ionization of Al by Ar ions. Even accounting for the fact that each projectile provides 13 electrons, the contribution expected from electron excitation is still not sufficient to explain the effect. (ii) The same phenomenon is not observed with S and Ar ions incident on Cl and K targets, nor with C^{+3}, O^{+2}, and Ne^{+3} ions incident on any of the targets.

2. *Excitation by secondary electrons.* During the passage of the projectile through the target, numerous secondary electrons (δ rays) are produced, some of which are sufficiently energetic to ionize target K-shell electrons. We have re-

TABLE VII. K- and L-shell vacancy filling fractions.

Atomic number	$\Gamma_{K\alpha}$ [a]	Γ_K [b] (eV)	Γ_L [c]	f_1	f_2
13	0.014	0.38	0.035	0.034	0.084
14	0.020	0.43	0.080	0.039	0.157
15	0.028	0.47	0.137	0.046	0.226
16	0.038	0.54	0.222	0.050	0.291
17	0.052	0.57	0.342	0.057	0.375
18	0.066	0.64	0.475	0.059	0.426
19	0.086	0.68	0.532	0.071	0.439
20	0.108	0.74	0.586	0.081	0.442

[a] From Ref. 31.

[b] $\Gamma_K = \Gamma_{K\alpha}/\omega_K$, where $\Gamma_{K\alpha}$ is from Ref. 31 and ω_K is from Ref. 19.

[c] From Ref. 32.

jected this mechanism for the following reasons: (i) Estimates of the magnitude of this effect based on the work of Jarvis *et al.*[34] indicate a contribution to the total x-ray yield of the order of 4% at most. (ii) The same phenomenon is not observed with S and Ar ions incident on Cl and K targets. In fact, the production of secondary electrons is expected to have approximately the same dependence on projectile charge as does the production of K x rays. Therefore, the relative yield of K x rays produced by secondary electrons should be essentially the same for *all* projectiles of the same velocity incident on the same target.

3. Electron promotion in target-atom recoil collisions. A most intriguing possibility is electron promotion as a result of quasimolecular level crossings during target-atom–target-atom collisions. These collisions could presumably occur as a result of large momentum transfers in close collisions between target atoms and projectiles. The highly ionized recoiling target atoms would carry vacancies into subsequent low-energy collisions with other target atoms which might be suitable for electron promotion from the K shells of the stationary target atoms. We have rejected this mechanism for the following reason: The cross section for the transfer of energy greater than a given amount $E_{\min}$ is given by[35]

$$\sigma_Q = \frac{2\pi}{M_2}\left(\frac{Z_1 Z_2 e^2}{V}\right)^2\left(\frac{1}{E_{\min}} - \frac{1}{E_{\max}}\right),$$

where M_2 is the mass of the target atom and V is the projectile velocity. Since this equation is only slightly dependent upon the mass of the projectile ($E_{\max}$ depends on the reduced mass), it is seen that σ_Q has essentially the same projectile charge dependence as does the K x-ray-production cross section. Therefore the relative contribution of this mechanism to the total K x-ray yield should be roughly the same for *all* projectiles of the same velocity incident on the same target. Moreover, estimates based on the energy required to bring two Al atoms to within a distance $2\bar{r}_K$ of each other, where $\bar{r}_K$ is the average K-shell radius, indicate that this mechanism could contribute at most only about 0.04% of the total K x-ray yield.

For lack of an alternative explanation, it would appear worthwhile to explore further the possibility that the $K\alpha_{1,2}$ intensity enhancement is *not* associated with a separate mechanism, but merely characterizes a new aspect of the direct Coulomb excitation process. For example, one would be led to expect this kind of effect if the $p_k(b)$ curve shown in Fig. 12 exhibited a second peak at impact parameters in the region where $p_L(b)$ is rapidly decreasing. Recent theoretical work by Reading and Fitchard does in fact provide some basis for the above hypothesis.[36,37] In simplified terms, their results indicate that a rise in $p_k(b)$ at large impact parameters might occur as a consequence of two competing effects. The electron velocity distribution favors ionization at small impact parameters, but at small impact parameters the effective electron binding energy is increased because of the combined attraction of the target and projectile nuclei. At large impact parameters, however, attraction to the projectile reduces the effective electron binding energy and enhances the ionization probability. When the projectile atomic number is comparable to that of the target, this latter effect could be of considerable importance. It is clear that further work aimed at investigating the energy and atomic-number dependences of the effect will be required before any substantive conclusions can be reached.

V. SUMMARY

Results of the present work have disclosed fairly large discrepancies between measured $K\alpha$ x-ray satellite energy differences for Cl and K, and those calculated by the Hartree-Fock-Slater method. It is felt that these discrepancies are attributable to (i) the inadequacy of the Slater exchange approximation, and (ii) additional energy increases associated with outer-shell ionization.

Evidence of level-matching effects was found in an examination of the projectile atomic-number dependence of the binomial probability parameter characterizing the $K\alpha$ satellite intensity pattern. Calculations of these probability parameters using the Coulomb ionization binary-encounter model yielded values which were much larger than those obtained experimentally, even for He-ion projectiles incident on Al where L-vacancy transfer effects are expected to be unimportant.

A striking departure from the usual binomial intensity pattern was observed in the $K\alpha$ spectra for S and Ar ions incident on Al. It was found that the $K\alpha_{1,2}$ peak intensity is considerably enhanced relative to the intensities of the various satellite peaks.

ACKNOWLEDGMENTS

We thank Dr. J. F. Reading for numerous discussions during the course of this work as well as T. L. Hardt and C. H. Rutledge for their help with the experiments and data analysis. We are grateful to Dr. D. J. Nagel for providing us with the basic spectrometer design and we acknowledge the assistance of D. S. Strack during the construction of the spectrometer. Our gratitude goes also to the operations staff of the Texas A & M Cyclotron Institute.

*Supported in part by the U. S. Atomic Energy Commission and the Robert A. Welch Foundation.

[1]A review covering this subject is given by J. D. Garcia, R. J. Fortner, and T. M. Kavanagh, Rev. Mod. Phys. 45, 111 (1973).
[2]A. R. Knudson, D. J. Nagel, P. G. Burkhalter, and K. L. Dunning, Phys. Rev. Lett. 26, 1149 (1971).
[3]Forrest Hopkins, D. O. Elliott, C. P. Bhalla, and Patrick Richard, Phys. Rev. A 8, 2952 (1973).
[4]D. Burch, Patrick Richard, and R. L. Blake, Phys. Rev. Lett. 26, 1355 (1971).
[5]D. G. McCrary and Patrick Richard, Phys. Rev. A 5, 1249 (1972).
[6]D. G. McCrary, M. Senglaub, and Patrick Richard, Phys. Rev. A 6, 263 (1972).
[7]D. Burch and H. Swanson, Proceedings of the International Conference on Inner-Shell Ionization Phenomena, Atlanta, 1972, Conf.-720404 (USAEC) Vol. 2, p. 1464.
[8]A. R. Knudson, P. G. Burkhalter, and D. J. Nagel, Proceedings of the International Conference on Inner-Shell Ionization, Atlanta, Ga., 1972 (U. S. AEC Conference No. 720404), Vol. 3, p. 1675 (unpublished).
[9]T. K. Li, R. L. Watson, and J. S. Hansen, Phys. Rev. A 8, 1258 (1973).
[10]Patrick Richard, R. L. Kauffman, J. H. McGuire, C. Fred Moore, and David K. Olsen, Phys. Rev. A 8, 1369 (1973).
[11]J. B. Marion and F. C. Young, *Nuclear Reaction Analysis Graphs and Tables* (North-Holland, Amsterdam, 1967), p. 34.
[12]Naval Research Laboratory, X-ray Optics Branch, Washington, D. C.
[13]P. G. Burkhalter, A. R. Knudson, D. J. Nagel, and K. L. Dunning, Phys. Rev. A 6, 2093 (1972).
[14]R. L. Watson, H. R. Bowman, and S. G. Thompson, Phys. Rev. 162, 1169 (1967).
[15]J. A. Bearden, Rev. Mod. Phys. 39, 78 (1967).
[16]E. Storm and H. I. Israel, Nucl. Data A 7, 565 (1970).
[17]T. K. Li and R. L. Watson, Phys. Rev. A 9, 1574 (1974).
[18]R. L. Watson, C. W. Lewis, and J. B. Natowitz, Nucl. Phys. A 154, 561 (1970).
[19]W. Bambynek, B. Crasemann, R. W. Fink, H.-U. Freund, H. Mark, C. D. Swift, R. E. Price, and P. V. Rao, Rev. Mod. Phys. 44, 716 (1972).
[20]A. R. Knudson, P. G. Burkhalter, and D. J. Nagel, Proceedings of the Fifth International Conference on Atomic Collisions, Gatlinburg, 1973 (to be published).
[21]F. Herman and S. Skillman, *Atomic Structure Calculations* (Prentice-Hall, Englewood Cliffs, N. J., 1963).
[22]E. H. Kennard and E. G. Ramberg, Phys. Rev. 46, 1040 (1934).
[23]H. E. White, *Introduction to Atomic Spectra* (McGraw-Hill, New York, 1934).
[24]F. C. Jundt and D. J. Nagel, Proceedings of the Fifth International Conference on Atomic Collisions, Gatlinburg, 1973 (to be published).
[25]D. J. Nagel (private communication).
[26]J. D. Garcia, Phys. Rev. A 1, 280 (1970).
[27]J. S. Hansen, Phys. Rev. A 8, 822 (1973).
[28]T. L. Hardt and R. L. Watson, Phys. Rev. A 7, 1917 (1973).
[29]E. Laegsgaard, J. V. Anderson, and L. C. Feldman, Phys. Rev. Lett. 29, 1206 (1972).
[30]T. K. Li, Ph.D. thesis (Texas A & M University, 1973) (unpublished).
[31]J. H. Scofield, Phys. Rev. 179, 9 (1969).
[32]E. J. McGuire, Phys. Rev. A 3, 587 (1971).
[33]A. M. Arthurs and B. L. Moiseiwitsch, Proc. R. Soc. Lond. A 247, 550 (1958).
[34]O. N. Jarvis, C. Whitehead, and M. Shah, Nuclear Physics Division, Atomic Energy Research Establishment (Harwell, Berkshire, England) Report No. AERE-R6612, 1970 (unpublished).
[35]R. D. Evans, *The Atomic Nucleus* (McGraw-Hill, New York, 1955), p. 849.
[36]J. F. Reading (private communication).
[37]J. F. Reading and E. Fitchard, Phys. Rev. A 10, 168 (1974).